Magnetic flux rope formation within a magnetosheath hot flow anomaly

H. Hasegawa,[1] H. Zhang,[2] Y. Lin,[3] B. U. Ö. Sonnerup,[4] S. J. Schwartz,[5] B. Lavraud,[6,7] and Q.-G. Zong[8,9]

Received 7 May 2012; revised 5 July 2012; accepted 6 August 2012; published 14 September 2012.

[1] We report observations on 1 March 2004 by the Cluster spacecraft of a hot flow anomaly (HFA) encountered in the dayside magnetosheath near Earth's bow shock. Embedded within the HFA was a magnetic flux rope with a diameter of a few thousand km, which was moving sunward and was presumably expanding. The pristine upstream solar wind seen by the ACE spacecraft contains an interplanetary current sheet favorable for the HFA formation, but shows no flux rope signatures. The properties of the flux rope, such as its slow speed, magnetic field variations, and the absence of magnetospheric electrons, are not likely to be due to magnetopause flux transfer events. These results suggest that the flux rope was created in the magnetosheath, rather than in the solar wind, in the foreshock, or on the magnetopause, through magnetic reconnection initiated in the course of the HFA development. Interestingly, energetic (~100 keV) electron fluxes were enhanced in and around this HFA-associated flux rope. The observations indicate that reconnection can occur within the magnetosheath part of HFAs and that such reconnection may play a role in electron acceleration, which is a common feature of HFAs.

Citation: Hasegawa, H., H. Zhang, Y. Lin, B. U. Ö. Sonnerup, S. J. Schwartz, B. Lavraud, and Q.-G. Zong (2012), Magnetic flux rope formation within a magnetosheath hot flow anomaly, *J. Geophys. Res.*, *117*, A09214, doi:10.1029/2012JA017920.

1. Introduction

[2] Hot flow anomalies (HFAs) are events observed near a planetary bow shock that are characterized by flows of heated solar wind plasmas deflected greatly from the Sun-Planet line [e.g., *Schwartz*, 1995]. They result from the interaction with the bow shock of an interplanetary current sheet, generally a tangential discontinuity (TD), when the motional electric field points toward the current sheet on at least one side [*Thomsen et al.*, 1993]. HFAs can be observed in the magnetosheath as well [e.g., *Paschmann et al.*, 1988; *Safrankova et al.*, 2002; *Eastwood et al.*, 2008] and, at Earth, have been shown to cause an outward displacement of the dayside magnetopause by about 5 R_E and significant auroral brightening [*Sibeck et al.*, 1999]. They can occur at a rate of several per day [*Schwartz et al.*, 2000] and thus may have significant effects on the geospace environment.

[3] HFAs were first discovered in the solar wind region immediately upstream of the Earth's bow shock, known as the foreshock, by the AMPTE [*Schwartz et al.*, 1985] and ISEE [*Thomsen et al.*, 1986] spacecraft. Recently, observations by the Cassini spacecraft have confirmed that HFAs can occur also near the bow shock of Saturn, another magnetized planet [*Masters et al.*, 2009]. HFAs are now known to form near the bow shock of an unmagnetized planet as well. *Øieroset et al.* [2001] reported observations by Mars Global Surveyor of a hot diamagnetic cavity upstream of the Martian bow shock, suggestive of the HFA formation at Mars. Most recently, evidence for HFAs in the Venusian foreshock has been presented by *Collinson et al.* [2012], who analyzed multi-instrument data taken by the Venus Express spacecraft.

[4] It is interesting that HFAs can be generated at Venus and Mars, where the size of the obstacle against the solar wind, i.e., of the ionosphere is only comparable to that of the planet itself, which is much smaller than the Earth's magnetosphere. This is because the facts indicate that, even at those unmagnetized planets, there is sufficient time for an interplanetary discontinuity to interact with the bow shock and to create an HFA. It is thus inferred that HFAs can occur essentially wherever a TD intersects and interacts with a collisionless shock under favorable conditions: HFAs may

[1]Institute of Space and Astronautical Science, JAXA, Sagamihara, Japan.
[2]Geophysical Institute, University of Alaska Fairbanks, Fairbanks, Alaska, USA.
[3]Physics Department, Auburn University, Auburn, Alabama, USA.
[4]Thayer School of Engineering, Dartmouth College, Hanover, New Hampshire, USA.
[5]Blackett Laboratory, Imperial College London, London, UK.
[6]Institut de Recherche en Astrophysique et Planétologie, Université de Toulouse, Toulouse, France.
[7]UMR 5277, Centre National de la Recherche Scientifique, Toulouse, France.
[8]Institute of Space Physics and Applied Technology, Peking University, Beijing, China.
[9]Center for Atmospheric Research, University of Massachusetts, Lowell, Massachusetts, USA.

Corresponding author: H. Hasegawa, ISAS/JAXA, 3-1-1 Yoshinodai, Chuo-ku, Sagamihara, Kanagawa 252-5210, Japan. (hase@stp.isas.jaxa.jp)

0148-0227/12/2012JA017920

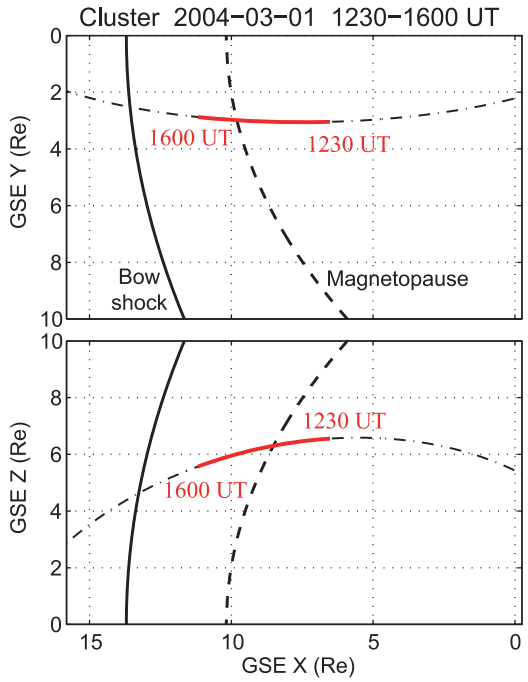

Figure 1. Trajectory in GSE coordinates of the Cluster 3 (C3) spacecraft on 1 March 2004, with the interval 1230–1600 UT shown in Figure 2 being highlighted by red curves. Model bow shock [*Farris et al.*, 1991] (solid curve) and magnetopause [*Roelof and Sibeck*, 1993] (dashed curve) positions are projected onto the GSE (top) *x*-*y* and (bottom) *x*-*z* planes. The bow shock position is an average and is shown only for reference.

well be a ubiquitous phenomenon in space and astrophysical plasmas.

[5] One outstanding question is how particles are accelerated and heated inside HFAs. The presence of energetic (>70 keV) electrons in HFAs has already been reported by *Paschmann et al.* [1988], who suggested that they were of magnetospheric origin. However, the nature of electron velocity distributions has received less attention than that of ions [e.g., *Schwartz*, 1995], although *Eastwood et al.* [2008] and *Zhang et al.* [2010] discussed the electron firehose and lower hybrid drift instabilities as the isotropization and heating processes within HFAs, respectively.

[6] Hybrid simulations of HFAs suggest that magnetic reconnection may be initiated as the TD interacts with the bow shock [*Lin*, 1997]. While it has been shown that reconnection can occur in a turbulent magnetosheath plasma downstream of the quasi-parallel bow shock [e.g., *Retinò et al.*, 2007] and in a magnetosheath current sheet compressed against the magnetopause [*Phan et al.*, 2011], there is to date no observational confirmation of the link between reconnection and HFAs. In this paper, we report Cluster spacecraft observations of a magnetic flux rope in the dayside magnetosheath, the presence of which is suggestive of reconnection initiated within magnetosheath HFAs.

[7] The paper is organized as follows. In section 2, an overview is given of ACE and Cluster observations on 1 March 2004, during which the magnetosheath HFA in question was encountered. In section 3, the results are presented from detailed analyses of the HFA and flux rope embedded in it. In section 4, discussion is given of the mechanism by which the magnetosheath flux rope is created and of an implication of the observations for electron acceleration near the bow shock.

2. Overview of the Observations

[8] In this paper, the ACE spacecraft is used as a monitor of upstream solar wind conditions, and data taken by the Cluster 3 (C3) spacecraft are presented, unless otherwise noted. The reason for this choice is that while both C1 and C3 usually provide full ion and magnetic field measurements, only C3 had no gap in the ion (CIS/HIA) measurements [*Rème et al.*, 2001] during the HFA encounter reported below. Note, however, that since the four Cluster spacecraft were separated by only 200–300 km during the observations, the data with time resolution of order 1 s were very similar among the four. This is indeed demonstrated by high time-resolution magnetic field measurements with the FGM instrument [*Balogh et al.*, 2001], as shown in Figure 5. Other data analyzed are of low-energy (1 eV to 25 keV) electrons from PEACE [*Johnstone et al.*, 1997] and of high-energy (20 to 400 keV) electrons from RAPID [*Wilken et al.*, 2001]. For PEACE, data from C4 are presented, because no data were available from C3 during the interval of interest.

[9] Figure 1 shows the C3 orbit on 1 March 2004 in GSE coordinates, along with model magnetopause and bow shock positions. The input parameters used in the magnetopause model [*Roelof and Sibeck*, 1993] are IMF $B_z = -2$ nT, solar wind speed $V_{sw} = 650$ km/s, and solar wind density $N_{sw} = 3$ cm^{-3}. Figure 2 shows that for the interval 1230–1600 UT, Cluster was initially in the dayside magnetosphere equatorward of the northern cusp, crossed the magnetopause a few times at around 1300 UT, traversed the magnetosheath in the northern hemisphere, and finally entered the upstream solar wind by crossing the bow shock at ~1552 UT.

[10] ACE, located at ~(219, −5, 0) R_E at 1500 UT, observed varying orientation of the IMF (Figure 2a) in a relatively high-speed solar wind (Figure 2b), which is a condition favorable for the HFA formation [*Facskó et al.*, 2008]. The fast magnetosonic Mach number was 6.4. Here, the time series of ACE data are shifted forward by 39 min such that the interplanetary discontinuity, resulting in the magnetosheath HFA analyzed in section 3, coincides with that seen by C3. The presence of the discontinuity is evident from an abrupt duskward turning of the field at ~1506 UT (marked by the green dashed line in Figure 2). The shift of 39 min may seem inconsistent with simple propagation in the $-x$ direction of the solar wind: It takes ~34 min for the observed flow with $V_x \sim -650$ km to travel from ACE to C3, which was at (10.0, 3.0, 6.0) R_E at 1500 UT. However, it actually agrees well with the propagation time ~40 min estimated by taking into account the separation between ACE and C3 in the *y*-*z* plane as well and the tilted orientation of the interplanetary discontinuity. Assuming that the discontinuity at 1506 UT is a planar TD, its normal is determined to be $\mathbf{n}_{TD} = (-0.224, 0.410, 0.884)$ from minimum variance analysis constrained to give the mean magnetic field component along the normal $\langle B_n \rangle = 0$ (MVABC) [*Sonnerup and Scheible*, 1998]. With this shift, the trend of temporal variations in the magnetosheath field direction seen by C3 (Figure 2c) is similar to that of the upstream IMF.

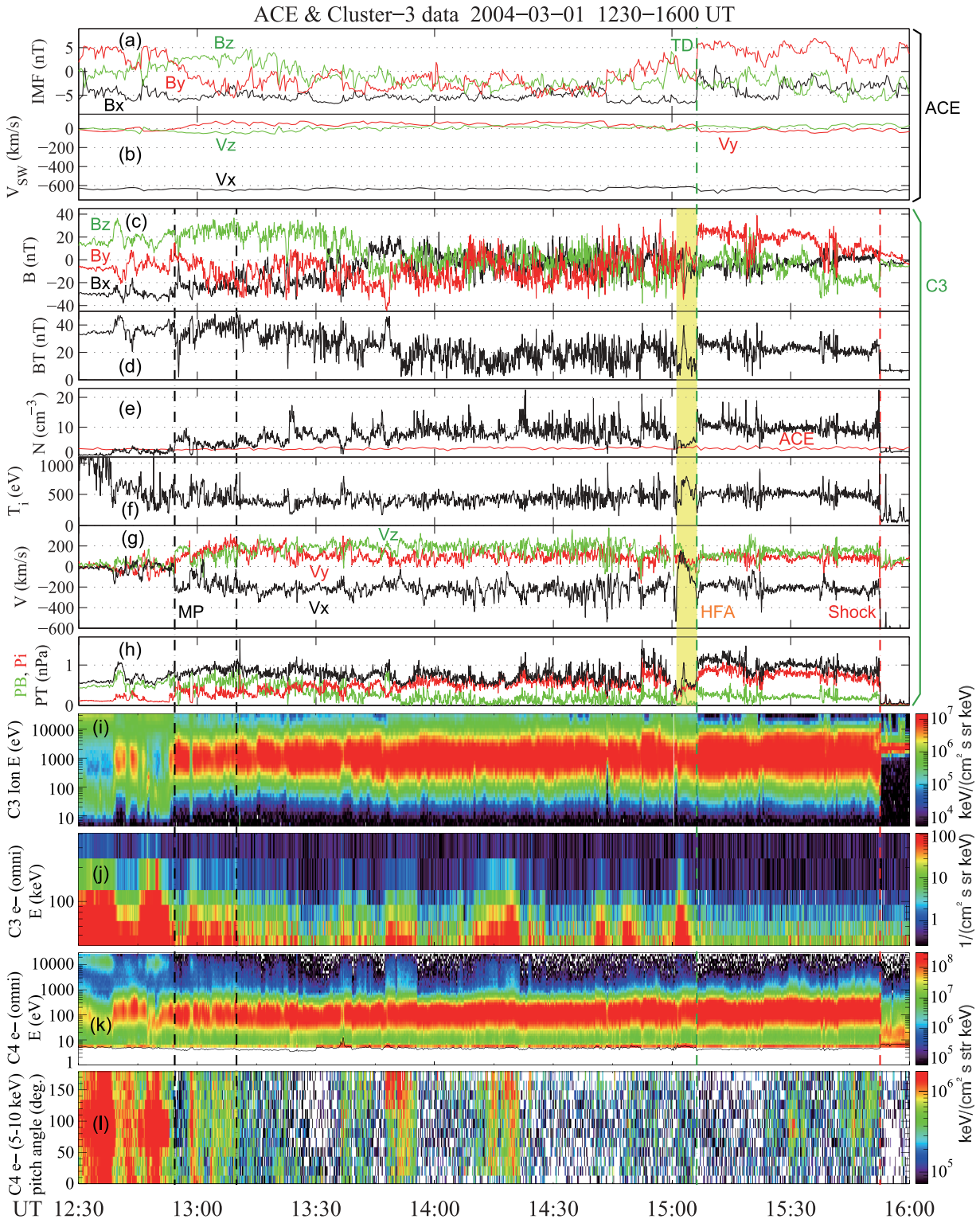

Figure 2. Data taken by the ACE spacecraft and C3 on 1 March 2004, 1230–1600 UT. (a, b) GSE components of the IMF and solar wind velocity seen by ACE, shifted forward by 39 min. (c, d) Magnetic field and (e–g) ion data taken by C3 (in Figure 2e, the ACE density is overlaid), and (h) magnetic (green), ion (red), and total (black) pressures. (i) Energy-time spectrogram of omni-directional differential energy fluxes (*JE*) of ions from the CIS/HIA instrument, (j) energetic electron fluxes from RAPID, (k) *JE* of omni-directional, low-energy electrons from PEACE, and (l) pitch angle distributions of 5–10 keV electrons. In Figures 2k and 2l, C4 data are shown because C3 data were not available. The first and final magnetopause crossings are marked by black dashed lines, and the bow shock crossing by a red dashed line. The interval of the magnetosheath hot flow anomaly (HFA) in question is shaded by yellow bar.

[11] The IMF prior to the TD crossing was largely dominated by the B_x component, while the IMF following the TD was by the B_y component (Figure 2a). As expected from these upstream conditions, the magnetic field and velocity before the TD crossing showed strong fluctuations downstream of the quasi-parallel bow shock, whereas the interval after the TD was characterized by relatively stable fields and velocities downstream of the quasi-perpendicular shock (Figures 2 and 2g). Consistent with such shock configurations, ions in the highest energy (>20 keV) range have a higher flux intensity before than after the TD crossing (Figure 2i) [e.g., *Retinò et al.*, 2007].

[12] Intermittent enhancements of high-energy (>20 keV) electron fluxes were observed during the magnetosheath interval between the final magnetopause and TD crossings (Figure 2j). For the flux enhancements before 1430 UT, electrons with energies 5–10 keV also had relatively high flux intensities, comparable to those of magnetospheric electrons observed earlier, and were streaming anti-parallel to the local magnetic field (e.g., at ∼1350 UT and ∼1420 UT in Figures 2k and 2l). These features can be explained by transient bursts of reconnection at the low-latitude magnetopause under weakly southward and anti-sunward IMF conditions, which results in leakage along reconnected field lines of magnetospheric particles into the magnetosheath. The observed anti-field-aligned fluxes suggest that Cluster encountered reconnected field lines on the northern side of a magnetopause X-line, which is also supported by the Cluster location. For those enhancements after 1430 UT, on the other hand, the lower-energy (5–10 keV) electrons had flux intensities which were higher than in the surrounding intervals but were not as high as during the earlier enhancements, and were more or less isotropic (Figure 2l). These later enhancements thus do not appear to be due to magnetopause reconnection.

[13] The HFA in question was observed during the interval 1501–1507 UT (shaded by yellow bar in Figure 2). It is seen that this HFA encounter occurred rather far from the magnetopause (marked by black dashed lines) and relatively close to the bow shock (red dashed line). Note that Cluster moved about 5 R_E sunward during the 3.5-hour interval under a roughly constant solar wind dynamic pressure condition (Figures 1 and 2). In the following, we focus on a shorter interval 1440–1515 UT, shown in Figure 3.

3. Analysis

3.1. Assessment of HFA Formation Conditions

[14] The interplanetary magnetic field components immediately before and after the TD crossing were (−6.6, −1.3, −1.1) nT and (−2.2, 5.4, −3.3) nT, respectively, with magnetic shear across the TD of 75.5°. For these field orientations, the shock angle at the nose of the nominal bow shock is $\theta_{Bn} \sim 14°$ and $\theta_{Bn} \sim 71°$, respectively. As required for the HFA formation, the motional electric field pointed toward the TD on both sides (Figure 4), satisfying equation (2) in *Thomsen et al.* [1993]. Such a configuration enables solar wind ions reflected from the bow shock into its upstream side to be channeled and accelerated toward the TD.

[15] In addition, the TD normal had a large cone angle ($\theta_{cs:sw} \sim 77°$) relative to the GSE x axis, allowing for the intersection between the current sheet and bow shock to move relatively slowly along the shock so that the kinetic processes inherent in the HFA formation can vigorously occur [*Schwartz et al.*, 2000]. Indeed, the ratio of the transit velocity of the discontinuity (V_{tr}) to the gyrovelocity of the reflected ion (V_g), defined as

$$\left|\frac{V_{tr}}{V_g}\right| = \frac{\cos\theta_{cs:sw}}{2\cos\theta_{bs:sw}\sin\theta_{Bn}\sin\theta_{cs:bs}}, \quad (1)$$

is less than unity, as required: the ratio is 0.46 and 0.12 for the shock angle before and after the TD crossing, respectively. Here, $\theta_{bs:sw}$ is the angle between the solar wind velocity and bow shock normal, and $\theta_{cs:bs}$ is the angle between the shock normal and normal to the interplanetary current sheet. It is thus seen that the upstream conditions were favorable for the HFA formation.

3.2. Properties of the HFA

[16] The magnetosheath HFA observed during the interval 1501–1507 UT shows typical features such as decreases in the density and field intensity (except for the flux rope interval discussed below), enhanced ion temperature (>500 eV), and strongly deflected and partially sunward flows (Figures 3d–3g) [*Schwartz et al.*, 2000, and references therein]. Note that the total (magnetic plus ion) pressure was lower in the HFA than in the surrounding magnetosheath regions (Figure 3h) (the ion to electron temperature ratio was ∼6 for the magnetosheath interval, so that the electron pressure can be neglected). This agrees with the property of a magnetosheath HFA seen in a global hybrid simulation [see *Lin*, 2002, Figure 5]. The reduced total pressure and sunward flow in the magnetosheath are also consistent with the expected outward displacement of the magnetopause as an HFA travels past the magnetosphere [*Sibeck et al.*, 1999]. A reduction in the magnetosheath total pressure causes a pressure imbalance at the magnetopause and in the magnetosheath region anti-sunward of the HFA, which can result in a sunward magnetosheath flow. In the present HFA, significant compressions of the field and plasma were seen only at its trailing edge (at ∼1507 UT) [e.g., *Schwartz*, 1995]. Moreover, this HFA appears to be on the side of the TD with a quasi-parallel shock configuration, in agreement with a global simulation by *Omidi and Sibeck* [2007] and earlier observations [*Facskó et al.*, 2009; *Zhang et al.*, 2010].

[17] Assuming planarity of the HFA boundaries, their orientation and motion are estimated from four-spacecraft timing analysis [e.g., *Schwartz*, 1998], applied to high time-resolution magnetic field data as shown in Figure 5. The normal to the leading boundary (at 1501:14 UT) is found to be $\mathbf{n}_{leading}$ = (0.047, 0.036, 0.998), and its velocity along the normal is $V_{n,leading}$ = 167.6 km/s, whereas for the trailing boundary (at 1506:15 UT), $\mathbf{n}_{trailing}$ = (−0.829, −0.095, 0.551) and $V_{n,trailing}$ = 181.8 km/s. These normals are compatible with those from MVABC: $\mathbf{n}_{Leading}$ = (−0.074, 0.061, 0.995) and $\mathbf{n}_{Trailing}$ = (−0.667, 0.211, 0.714). The results indicate that the HFA was generally moving northward, consistent with the orientation of the upstream TD (section 2).

[18] Observed between these HFA boundaries was a magnetic flux rope, whose signatures are bipolar variations in B_x and B_z, and peaked field intensity and total pressure (between dash-dotted lines in Figures 3c, 3d, 3h, and 5). The presence of a flux rope is further confirmed in subsection 3.3.

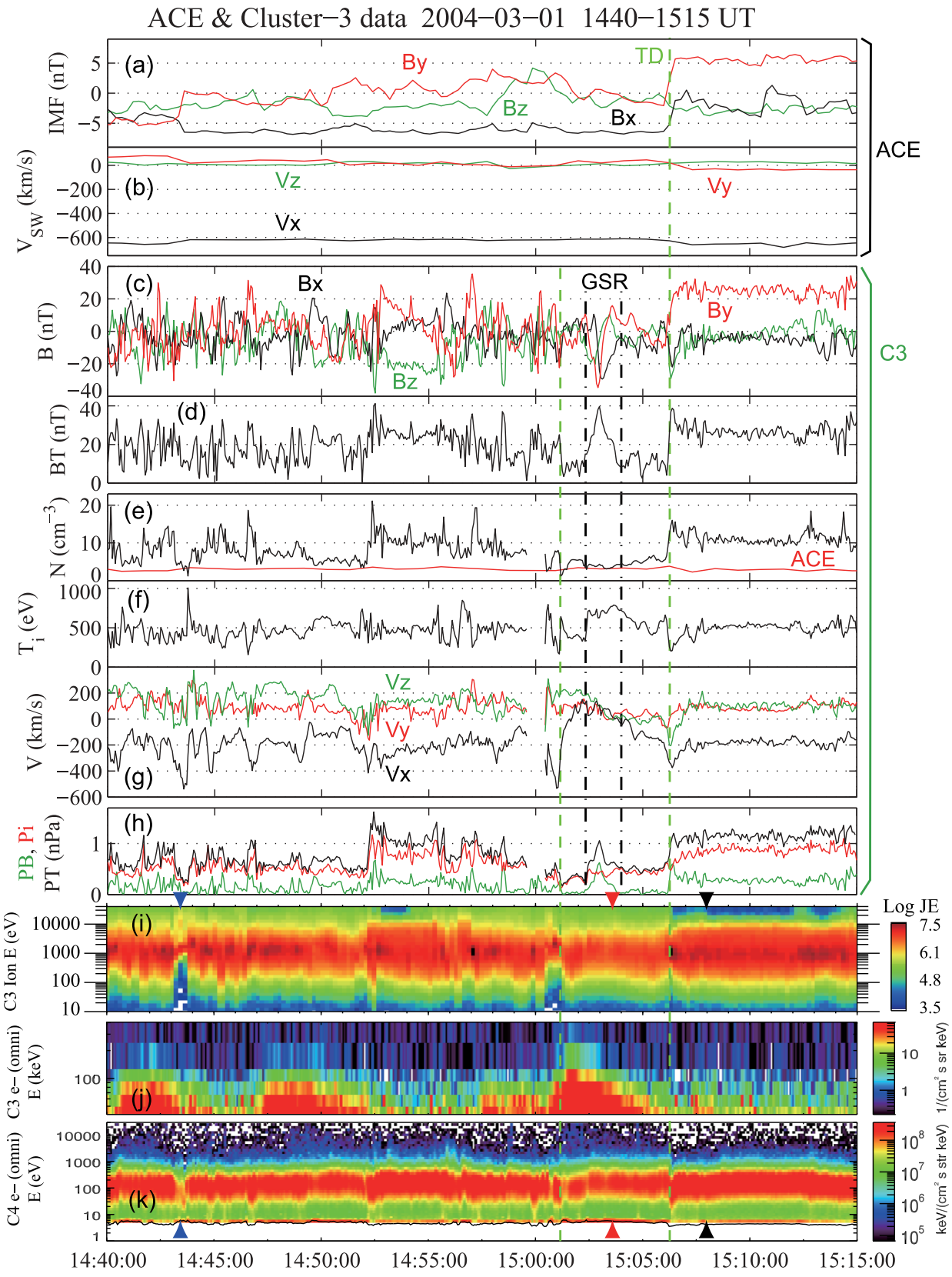

Figure 3. (a–k) Data taken by ACE and C3 on 1 March 2004, 1440–1515 UT, with the same format as in Figure 2 (except that there is no panel for electron pitch angle distributions). The intervals of the magnetosheath HFA and of Grad-Shafranov reconstruction (GSR) are sandwiched by two green and black vertical lines, respectively. Triangles in Figures 3i and 3k mark the times when particle velocity/energy distributions in Figure 6 were recorded.

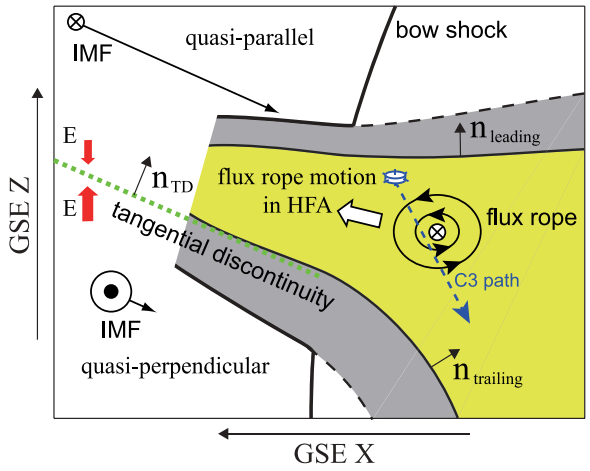

Figure 4. Schematic drawing of the magnetosheath HFA seen by Cluster. The C3 path is shown in a frame of reference moving with the flux rope (i.e., the HT frame), for easier comparison with Figures 7c and 7d. The HFA generally moved northward in the Earth's rest frame, while the flux rope moved sunward in the HFA rest frame.

Note that no such flux rope signatures were seen by ACE (Figure 3a), which indicates that the flux rope was created near or downstream of the bow shock.

[19] Figure 6 shows two-dimensional (2D) cuts in velocity and energy space of phase space densities of ions and electrons, respectively, in the HFA, in the magnetosheath downstream of the quasi-perpendicular shock, and in the foreshock. Ions in the HFA were hot and isotropic, while ions in the other regions had an anisotropy or consisted of two populations (Figures 6a–6c). Electrons in the HFA were also isotropic and had higher fluxes at ~1 keV than in the other regions (Figures 6d–6f). Note also that electrons with energies ≥1 keV can be expressed by a power law, i.e., they appear to be a nonthermal component. These features indicate that the observed HFA was mature, rather than young [*Zhang et al.*, 2010]. The observed location (in the northern hemisphere) and northward motion of the HFA also support that there was sufficient time for the HFA to become mature before it was encountered, since the TD began to interact with the bow shock in the southern hemisphere.

3.3. Grad-Shafranov Reconstruction

[20] Figure 7 shows results from Grad-Shafranov reconstruction (GSR) [*Sonnerup and Guo*, 1996; *Hasegawa et al.*, 2004] applied to C3 data for the flux rope interval 1502:22–1503:59 UT, assuming that the structure is 2D and magnetohydrostatic (see Appendix A for the methodology). In Figures 7c and 7d, the field lines projected onto the GSR *x*-*y* plane, i.e., the transverse field lines are represented by equivector potential contour lines. From the deHoffmann-Teller (HT) analysis [*Khrabrov and Sonnerup*, 1998], the HT velocity is determined to be $\mathbf{V}_{HT}$ = (68.6, 26.7, 71.8) km/s, i.e., the flux rope was moving sunward and northward. The correlation coefficient between the three components of the convection electric field measured in the spacecraft-rest frame and those based on the HT velocity is 0.832; the HT frame is not determined very well, presumably because the flux rope was still evolving or expanding. This is inferred from the fact that the velocity components left over in the estimated HT frame are not strictly field-aligned but are generally directed away from the flux rope center (Figure 7d)

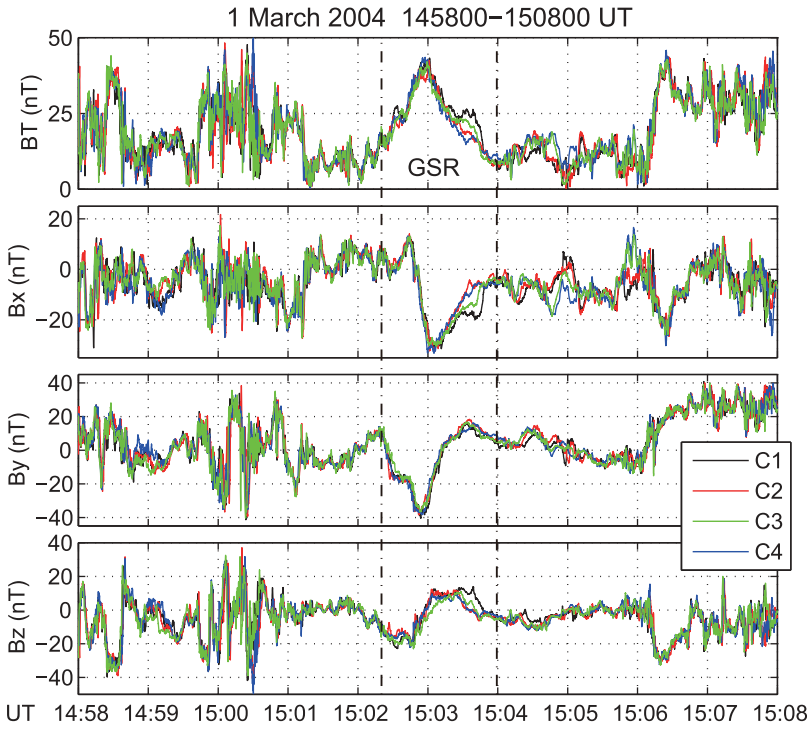

Figure 5. High time (22 Hz) resolution magnetic field data from the four Cluster spacecraft in GSE coordinates for the interval 1458–1508 UT. The GSR interval is sandwiched by two vertical dash-dotted lines.

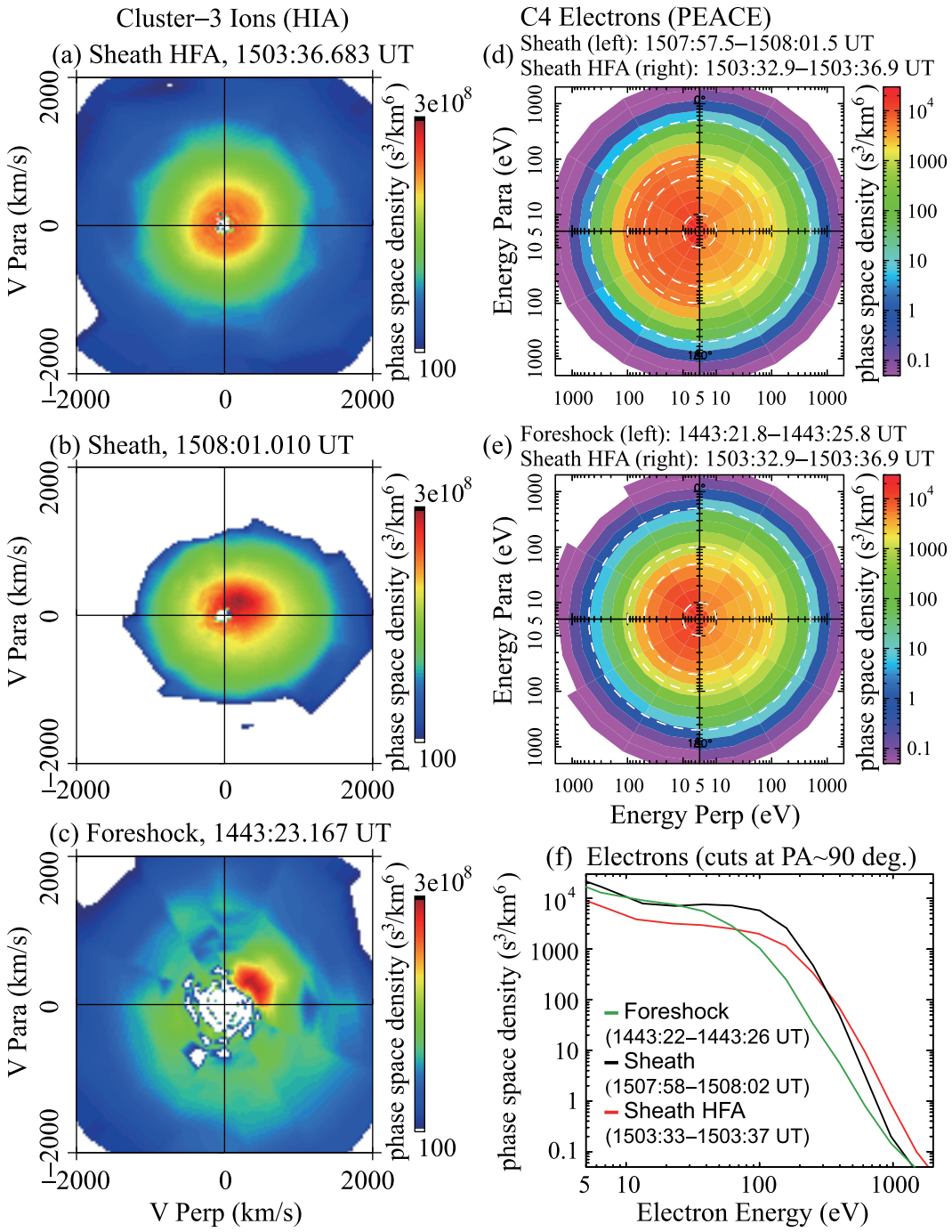

Figure 6. (a–c) Ion velocity distributions taken in the magnetosheath HFA, magnetosheath downstream of the quasi-perpendicular bow shock, and a foreshock region, respectively. Comparison of electron energy distributions (d) between the magnetosheath (left half) and HFA (right half) and (e) between the foreshock and HFA. (f) Electron phase space densities cut at pitch angle 90°, plotted as a function of energy.

(the assumption here is that the flux rope center was not accelerating/decelerating, but moved at a constant velocity).

[21] The invariant (GSR z) axis, along which no spatial gradient is assumed, is determined to be z = (0.390, 0.773, −0.501), through optimization of the correlation coefficient (0.981) between the three components of the magnetic field actually measured by C1, C2, and C4 and those predicted from the GSR map along the paths of the three spacecraft [*Hasegawa et al.*, 2004]. In 2D Grad-Shafranov equilibria, the transverse pressure P_t and axial field B_z should be preserved along the field lines; Figures 7a and 7b show that the data points can be fitted by single curves (thick solid curves), suggesting that the observed structure was approximately 2D. The invariant axis, parallel to the flux rope axis, has an angle of 117° with $\mathbf{n}_{leading}$ and of 132° with $\mathbf{n}_{trailing}$, and thus, as expected, is more perpendicular than parallel to the

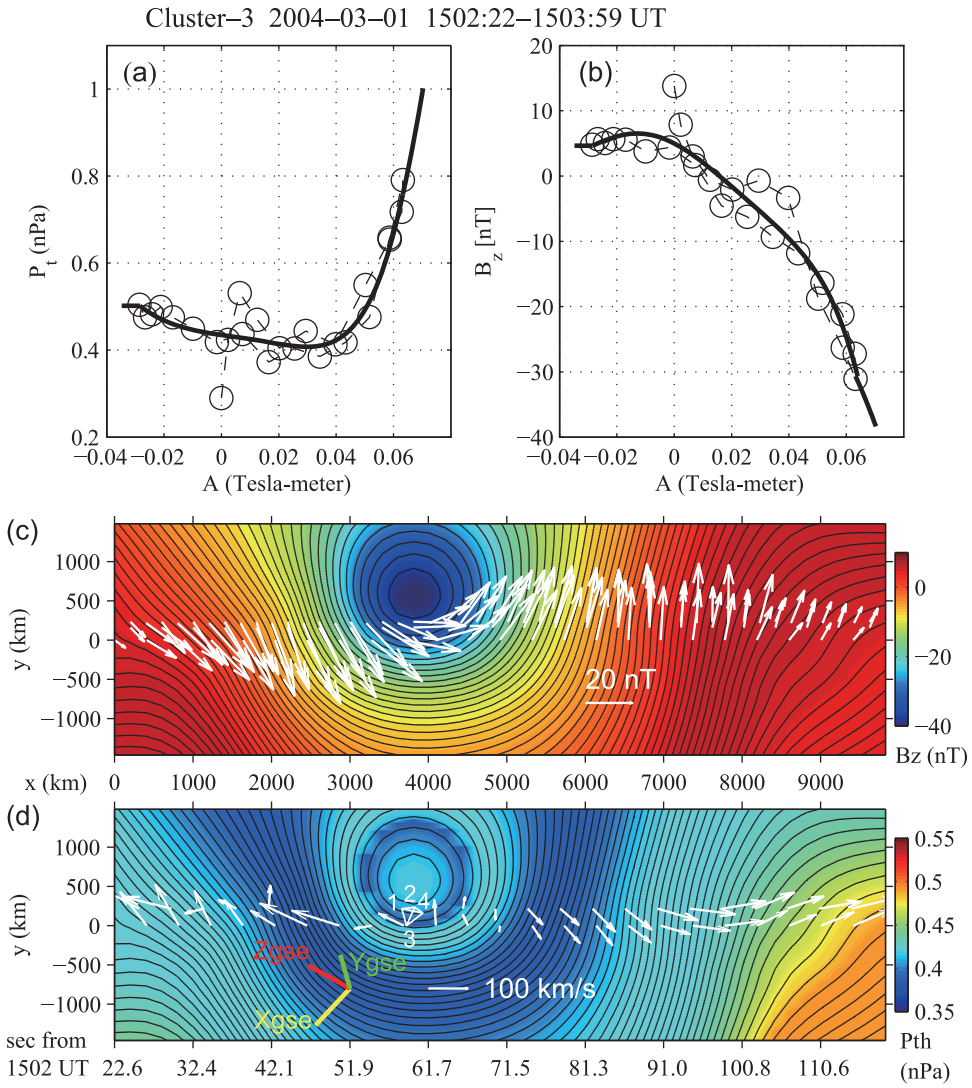

Figure 7. Results from Grad-Shafranov reconstruction using C3 data. (a) Transverse pressure ($P_t = p + B_z^2/(2\mu_0)$) and (b) axial magnetic field B_z, plotted as a function of the partial vector potential A. Open circles are the measurements and thick solid curves denote the fitted polynomials. (c, d) The reconstructed transverse field lines, with B_z in color in Figure 7c and the plasma pressure p in Figure 7d. The spacecraft moved (time progressed) from left to right. White arrows show the transverse field components measured by the four spacecraft in Figure 7c, and the measured velocity components from C1 and C3, transformed into the HT frame and projected onto the GSR x-y plane, in Figure 7d. The yellow, green, and red bars are the projections of the GSE x, y, and z axes, respectively.

HFA boundary normals. Moreover, the angle between the GSR z axis and upstream TD normal is 102.3° (i.e., they are roughly perpendicular). These results suggest that the flux rope was embedded in the magnetosheath HFA (Figure 4). It is concluded from Figure 7 that a flux rope with a diameter of a few thousand km existed between the HFA boundaries.

3.4. Properties of the Flux Rope

[22] Here we discuss, based on the properties of the flux rope observed in the HFA, where it originated from: the foreshock, magnetosheath, or magnetopause. The sunward motion of the flux rope indicates that it formed on the anti-sunward side of Cluster, i.e., within the magnetosheath or on the magnetopause. On the other hand, the brief excursion to the foreshock at ~1443 UT, only about 20 min before the HFA encounter, suggests that the flux rope was observed closer to the bow shock, rather than to the magnetopause. (This brief excursion may be associated with another interplanetary current sheet at ~1443 UT (Figure 3a).) Note also that around the time of the HFA encounter, the IMF was weakly southward on average, so that the nominal magnetopause location must have been even closer to the Earth than during the earlier northward IMF interval when Cluster crossed the magnetopause [e.g., *Sibeck et al.*, 1991].

[23] The orientation of the flux rope axis is roughly perpendicular (~102°) to the magnetopause normal $\mathbf{n}_{MP}$ = (0.617, −0.068, 0.784), estimated with MVABC for a magnetopause interval 1252:30–1255:00 UT (Figure 2). It is therefore in principle possible that the flux rope was embedded in the magnetopause. However, the northward

component of the flux rope velocity (the z component 71.8 km/s of $\mathbf{V}_{HT}$) is rather small, which is unlikely if the flux rope was part of the high-latitude but equatorward-of-the-cusp magnetopause and was swept poleward by a high-speed reconnection jet. In particular, even during the latter half of the flux rope interval (1503:00–1503:40 UT), when B_z was positive and thus which might possibly be the magnetospheric side of the magnetopause, V_z was very small and, importantly, smaller than in the surrounding magnetosheath region (Figures 3c and 3g). Since the latter interval corresponds to the equatorward and earthward side of the flux rope (Figure 4), a fast northward flow would be expected if the observations were made on this side of a high-latitude flux transfer event (FTE) [e.g., *Hasegawa et al.*, 2006]. Note also that B_y was positive during the latter interval (Figure 5), which is not expected if Cluster was in the duskside northern magnetosphere where B_y was negative (Figure 2c).

[24] We then discuss another possibility of magnetopause origin: an FTE flux rope was anchored in the ionosphere at both ends, causing it to move only slowly compared to the magnetosheath flow at these high latitudes, and a part of the rope was sucked off from the magnetopause into the magnetosheath by the lower total pressure in the HFA. While the isotropic nature of electrons inside the flux rope (Figures 6d and 6e) is in principle consistent with such a scenario of closed magnetic topology, the relatively low flux intensity of 5–10 keV electrons (Figure 2) does not seem to be consistent. Future studies, perhaps global hybrid simulations, may be able to answer if an HFA development can lead to emergence fully into the magnetosheath of a segment of an FTE flux rope.

[25] In summary, the observations are most consistent with the view that the flux rope was created through magnetic reconnection initiated somewhere within the magnetosheath part of the HFA, rather than in the foreshock or on the magnetopause. Its possibly ongoing expansion (subsection 3.3 and Figure 7d) suggests that it formed relatively recently in the course of the HFA formation or evolution. Figure 4 summarizes an approximate geometry of the structures observed in and around the HFA.

4. Discussion

[26] Figures 2j and 3j interestingly show that for electrons with energies ≥100 keV, the highest fluxes during the whole magnetosheath interval occurred at ∼1502 UT immediately before the flux rope encounter within the HFA. This is striking considering that the fluxes of the lower-energy (5–10 keV) electrons were lower during the HFA interval than the intervals before 1430 UT when energetic electron bursts likely due to magnetopause reconnection were observed. It indicates that a larger number of energetic (∼100 keV) electrons existed within the HFA than in the surrounding regions. Although part of these energetic electrons may have resulted from acceleration at and/or downstream of the quasi-parallel bow shock, the above correspondence suggests a link between the flux rope formation and energetic electrons in the HFA. Reconnection within the HFA may have led to the generation of these energetic electrons, in contrast with an earlier interpretation that energetic electrons in HFAs are of magnetospheric origin [*Paschmann et al.*, 1988]. We also note that the energetic electron fluxes were higher on the sunward, rather than on the anti-sunward, side of the sunward-moving flux rope. While the precise mechanism of electron acceleration or trapping to account for such a feature is an issue left for future study, the TD-shock interaction region appears to be a potentially important site of particle acceleration, as well as the shock-shock interaction region [e.g., *Hietala et al.*, 2011].

[27] The present observations are essentially consistent with hybrid simulations of HFAs in which reconnection occurs in association with the HFA generation [*Lin*, 1997]. Since the normals of interplanetary TDs resulting in HFAs have a large cone angle [*Schwartz et al.*, 2000], the current sheets would not be compressed as strongly when they cross the bow shock as in the situations of magnetosheath reconnection reported earlier [*Phan et al.*, 2007]. A question thus arises: How can reconnection be triggered in magnetosheath HFAs? This is also closely related to the question of exactly where reconnection was initiated: Was it closer to the bow shock or to the magnetopause, and was it within the TD or on the side with the quasi-parallel shock configuration where current sheets can be created in a turbulent magnetosheath plasma [*Retinò et al.*, 2007]?

[28] Since both Cluster observations (subsection 3.2) and the timing of the TD crossing (section 2) support that the flux rope as well as the HFA was encountered on the side with the quasi-parallel shock configuration, reconnection in this particular case may have occurred in a magnetosheath current sheet downstream of the quasi-parallel bow shock. The core field inside the flux rope was oriented roughly in the $-y$ direction (Figure 5 and subsection 3.3), opposite to the field direction after the TD crossing. This also seems to suggest that reconnection was triggered within a turbulent magnetosheath downstream of the quasi-parallel shock, rather than in the TD itself.

[29] We note that the ion temperature and density in HFAs are higher and lower, respectively, i.e., both the ion gyroradius and inertia length are larger, than in the surrounding magnetosheath regions (Figure 3 and also see *Paschmann et al.* [1988]). It is also speculated that a current sheet within magnetosheath HFAs may be compressed as it is pushed against the probably outward-moving dayside magnetopause [*Sibeck et al.*, 1999]. It thus may be that as an HFA develops, a current sheet in the magnetosheath part of the HFA becomes thinner relative to the characteristic length scales of ions, leading to the condition favorable for fast reconnection. Such reconnection may possibly be more efficient than in the magnetosheath region not affected by the HFA, as reported by *Retinò et al.* [2007], and may account for the substantial size (≥3000 km) of the flux rope and larger amount of energetic electrons.

[30] It is also likely that the current sheet is compressed more strongly at its part closer to, rather than farther from, the magnetopause [*Phan et al.*, 2011]: the reconnection rate may well be higher at an X-line nearer to the magnetopause. Such location-dependent reconnection may have pushed the resulting flux rope sunward and have enhanced the sunward flow in the magnetosheath HFA. If this is the case, the possibly observed expansion of the flux rope may be a combined effect of still ongoing reconnection (increasing magnetic flux content in the flux rope) and its motion toward the outer magnetosheath part where the total pressure would be lower than in the magnetosheath region closer to the

magnetopause. Further studies, e.g., using global three-dimensional kinetic simulations [e.g., *Pang et al.*, 2010], are necessary to address these questions of how and where within a magnetosheath HFA magnetic reconnection may initiate and how particles may be accelerated in the course of the HFA development.

Appendix A: Grad-Shafranov Reconstruction Technique

A1. Basics of Grad-Shafranov Reconstruction

[31] The Grad-Shafranov Reconstruction (GSR) technique (see, e.g., *Sonnerup et al.* [2008] for a review) recovers two-dimensional (2D), magneto-hydrostatic structures in space using, as spatial initial values, plasma and magnetic field data recorded as the structure moves past a single spacecraft. The equation governing the reconstruction is $\mathbf{j} \times \mathbf{B} = \nabla p$, which is derived from the MHD equation of motion by neglecting the inertia terms and which represents the balance between magnetic tension and the force from the total pressure gradient. Assuming that there is no spatial gradient along what we call the invariant axis ($\partial/\partial z \sim 0$), this force balance equation can be reduced to the Grad-Shafranov (GS) equation in a Cartesian coordinate system [e.g., *Sonnerup et al.*, 2006]:

$$\nabla^2 A = \frac{\partial^2 A}{\partial x^2} + \frac{\partial^2 A}{\partial y^2} = -\mu_0 \frac{dP_t(A)}{dA} \tag{A1}$$

where A is the partial vector potential (z component of the magnetic vector potential), so that the magnetic field is $\mathbf{B} = \nabla A \times \hat{\mathbf{z}} + B_z\hat{\mathbf{z}}$ or $(B_x, B_y, B_z) = [\partial A/\partial y, -\partial A/\partial x, B_z(A)]$. The transverse pressure $P_t(A) = p(A) + B_z^2(A)/(2\mu_0)$, plasma pressure $p(A)$, and axial field $B_z(A)$ are all constant along the transverse field lines; this property can be used to estimate the orientation of the invariant (GSR z) axis, when same field lines, characterized by equal A values, are encountered more than once along the path of the observing probe during the interval chosen for the reconstruction [*Hu and Sonnerup*, 2002]. See subsection A3 for how the invariant axis orientation is determined in the present study.

[32] For the reconstruction of the magnetic field in a rectangular domain in the GSR x-y plane, the GS equation is solved numerically by using the magnetic field measurements along the spacecraft path ($y = 0$ in the x-y plane) as spatial initial values [*Sonnerup and Guo*, 1996; *Hau and Sonnerup*, 1999]. This is usually performed in the deHoffmann-Teller (HT) frame discussed in subsection A2. The integration of A and B_x in the $\pm y$ directions uses the following (second and first order) Taylor series

$$A(x, y \pm \Delta y) = A(x, y) \pm \Delta y \frac{\partial A(x, y)}{\partial y} + \frac{1}{2}(\Delta y)^2 \frac{\partial^2 A(x, y)}{\partial y^2}, \tag{A2}$$

and

$$B_x(x, y \pm \Delta y) = B_x(x, y) \pm \Delta y \frac{\partial B_x(x, y)}{\partial y}, \tag{A3}$$

respectively. Here $\partial A(x, y)/\partial y = B_x$ is known and $\partial^2 A(x, y)/\partial y^2 = \partial B_x(x, y)/\partial y = -\partial^2 A(x, y)/\partial x^2 - \mu_0 dP_t/dA$ is taken from the GS equation (A1). The integration is stopped at certain y points, which define the y boundaries of the reconstruction domain. The transverse field, $\mathbf{B}_t = \nabla A \times \hat{\mathbf{z}}$, in the GSR x-y plane is then represented by equi-A contour lines (A is constant along the transverse field lines). The axial field and pressure in the maps are computed by use of the functions $B_z(A)$ and $p(A)$, which become available by determining a polynomial (or exponential) functional relationship between actually measured B_z and $A(x, 0)$ and between measured p and $A(x, 0)$, respectively, for the analyzed interval [*Hau and Sonnerup*, 1999] (see Figures 7a and 7b for an example). Here $A(x, 0)$ is calculated from spatial integration of measured B_y ($= -\partial A/\partial x$) along the spacecraft path (x axis).

A2. Frame Velocity Determination

[33] The reconstruction needs to be conducted in a proper frame of reference in which the structure, or at least its central part, such as the center of a magnetic island/flux rope, looks stationary. Determination of such a frame velocity allows for time series of data taken during an interval (temporal information) to be converted into spatial information at points along the spacecraft path. If the configuration of individual magnetic field lines does not vary significantly in time, the deHoffmann-Teller (HT) velocity, $\mathbf{V}_{HT}$, determined by a least squares technique described, e.g., by *Khrabrov and Sonnerup* [1998], can be used as the co-moving frame velocity. In the ideal HT frame, the plasma flow velocities should be strictly field-aligned so that the convection electric fields are exactly zero. In practice, non-negligible electric fields or perpendicular components of the velocity may remain, e.g., when the structure is evolving with time in the estimated HT frame (see Figure 7d for an example).

A3. Coordinate Axis Determination

[34] For successful reconstruction of 2D structures, not only the frame velocity but also proper coordinate axes need to be determined. The key orientation is that of the invariant (GSR z) axis along which gradients are assumed to be negligible. This axis can be estimated, with the method developed by *Hasegawa et al.* [2004], in such a way that the correlation coefficient between three components of the magnetic field actually measured by three of the four Cluster spacecraft that are not used for the reconstruction and those predicted from the GSR field map (Figure 7c) at points along the paths of the three spacecraft is maximized. Once the invariant axis orientation is chosen, the GSR x axis is defined to be anti-parallel to the projection of the HT velocity, $\mathbf{V}_{HT}$, onto the GSR x-y plane which is perpendicular to the GSR z axis; the GSR y axis completes the right-handed orthogonal system. The GSR x axis (or $y = 0$) thus represents the path of the observing spacecraft in the GSR x-y frame. The dimension of the reconstruction domain in the GSR x direction is $L_x = |V_{HTx}|(T_{en} - T_{st})$, where T_{st} and T_{en} are the start and end times, respectively, of the data interval in question and V_{HTx} is the GSR x component of the HT velocity, $V_{HTx} = (\mathbf{V}_{HT} \cdot \hat{\mathbf{z}}) - \mathbf{V}_{HT}$.

[35] **Acknowledgments.** We acknowledge the Cluster instrument (CIS, FGM, PEACE, and RAPID) teams. Some of the data were provided via the Cluster Active Archive (http://caa.estec.esa.int). H.H. thanks Adam Masters for helpful comments. H. Zhang and Q.-G. Zong acknowledge NSF grants AGS-1007449, AGS-0963111, and AGS-0962815.

[36] Philippa Browning thanks the reviewers for their assistance in evaluating this paper.

References

Balogh, A., et al. (2001), The Cluster magnetic field investigation: Overview of in-flight performance and initial results, *Ann. Geophys.*, *19*, 1207–1217.

Collinson, G. A., et al. (2012), Hot flow anomalies at Venus, *J. Geophys. Res.*, *117*, A04204, doi:10.1029/2011JA017277.

Eastwood, J. P., et al. (2008), THEMIS observations of a hot flow anomaly: Solar wind, magnetosheath, and ground-based measurements, *Geophys. Res. Lett.*, *35*, L17S03, doi:10.1029/2008GL033475.

Facskó, G., K. Kecskeméty, G. Erdös, M. Tátrallyay, P. W. Daly, and I. Dandouras (2008), A statistical study of hot flow anomalies using Cluster data, *Adv. Space Res.*, *41*, 1286–1291, doi:10.1016/j.asr.2008.02.005.

Facskó, G., Z. Németh, G. Erdös, A. Kis, and I. Dandouras (2009), A global study of hot flow anomalies using Cluster multi-spacecraft measurements, *Ann. Geophys.*, *27*, 2057–2076.

Farris, M. H., S. M. Petrinec, and C. T. Russell (1991), The thickness of the magnetosheath: Constraints on the polytropic index, *Geophys. Res. Lett.*, *18*, 1821–1824.

Hasegawa, H., et al. (2004), Reconstruction of two-dimensional magnetopause structures from Cluster observations: Verification of method, *Ann. Geophys.*, *22*, 1251–1266.

Hasegawa, H., B. U. Ö. Sonnerup, C. J. Owen, B. Klecker, G. Paschmann, A. Balogh, and H. Rème (2006), The structure of flux transfer events recovered from Cluster data, *Ann. Geophys.*, *24*, 603–618.

Hau, L.-N., and B. U. Ö. Sonnerup (1999), Two-dimensional coherent structures in the magnetopause: Recovery of static equilibria from single-spacecraft data, *J. Geophys. Res.*, *104*, 6899–6917.

Hietala, H., N. Agueda, K. Andreeova, R. Vainio, S. Nylund, E. K. J. Kilpua, and H. E. J. Koskinen (2011), In situ observations of particle acceleration in shock-shock interaction, *J. Geophys. Res.*, *116*, A10105, doi:10.1029/2011JA016669.

Hu, Q., and B. U. Ö. Sonnerup (2002), Reconstruction of magnetic clouds in the solar wind: Orientation and configuration, *J. Geophys. Res.*, *107*(A7), 1142, doi:10.1029/2001JA000293.

Johnstone, A. D., et al. (1997), PEACE: A Plasma Electron And Current Experiment, *Space Sci. Rev.*, *79*, 351–398, doi:10.1023/A:1004938001388.

Khrabrov, A. V., and B. U. Ö. Sonnerup (1998), DeHoffmann-Teller analysis, in *Analysis Methods for Multi-Spacecraft Data*, edited by G. Paschmann and P. W. Daly, chap. 9, pp. 221–248, Int. Space Sci. Inst., Bern, Switzerland.

Lin, Y. (1997), Generation of anomalous flows near the bow shock by its interaction with interplanetary discontinuities, *J. Geophys. Res.*, *102*(A11), 24,265–24,281.

Lin, Y. (2002), Global hybrid simulation of hot flow anomalies near the bow shock and in the magnetosheath, *Planet. Space Sci.*, *50*, 577–591.

Masters, A., et al. (2009), Hot flow anomalies at Saturn's bow shock, *J. Geophys. Res.*, *114*, A08217, doi:10.1029/2009JA014112.

Øieroset, M., D. L. Mitchell, T.-D. Phan, R. P. Lin, and M. H. Acuña (2001), Hot diamagnetic cavities upstream of the Martian bow shock, *Geophys. Res. Lett.*, *28*, 887–890.

Omidi, N., and D. G. Sibeck (2007), Formation of hot flow anomalies and solitary shocks, *J. Geophys. Res.*, *112*, A01203, doi:10.1029/2006JA011663.

Pang, Y., Y. Lin, X. H. Deng, X. Y. Wang, and B. Tan (2010), Three-dimensional hybrid simulation of magnetosheath reconnection under northward and southward interplanetary magnetic field, *J. Geophys. Res.*, *115*, A03203, doi:10.1029/2009JA014415.

Paschmann, G., G. Haerendel, N. Sckopke, E. Möbius, H. Lühr, and C. W. Carlson (1988), Three-dimensional plasma structures with anomalous flow directions near the Earth's bow shock, *J. Geophys. Res.*, *93*(A10), 11,279–11,294.

Phan, T. D., G. Paschmann, C. Twitty, F. S. Mozer, J. T. Gosling, J. P. Eastwood, M. Øieroset, H. Rème, and E. A. Lucek (2007), Evidence for magnetic reconnection initiated in the magnetosheath, *Geophys. Res. Lett.*, *34*, L14104, doi:10.1029/2007GL030343.

Phan, T. D., T. E. Love, J. T. Gosling, G. Paschmann, J. P. Eastwood, M. Oieroset, V. Angelopoulos, J. P. McFadden, D. Larson, and U. Auster (2011), Triggering of magnetic reconnection in a magnetosheath current sheet due to compression against the magnetopause, *Geophys. Res. Lett.*, *38*, L17101, doi:10.1029/2011GL048586.

Rème, H., et al. (2001), First multispacecraft ion measurements in and near the Earth's magnetosphere with the identical Cluster ion spectrometry (CIS) experiment, *Ann. Geophys.*, *19*, 1303–1354.

Retinò, A., et al. (2007), In situ evidence of magnetic reconnection in turbulent plasma, *Nat. Phys.*, *3*, 235–238, doi:10.1038/nphys574.

Roelof, E. D., and D. G. Sibeck (1993), Magnetopause shape as a bivariate function of interplanetary magnetic field B_z and solar wind dynamic pressure, *J. Geophys. Res.*, *98*, 21,421–21,450.

Safrankova, J., L. Prech, Z. Nemecek, and D. G. Sibeck (2002), The structure of hot flow anomalies in the magnetosheath, *Adv. Space Res.*, *30*(12), 2737–2744.

Schwartz, S. J. (1995), Hot flow anomalies near the Earth's bow shock, *Adv. Space Res.*, *15*, 107–116.

Schwartz, S. J. (1998), Shock and discontinuity normals, Mach numbers, and related parameters, in *Analysis Methods for Multi-Spacecraft Data, Sci. Rep. SR-001*, edited by G. Paschmann and P. W. Daly, chap. 10, pp. 249–270, Int. Space Sci. Inst., Bern, Switzerland.

Schwartz, S. J., et al. (1985), An active current sheet in the solar-wind, *Nature*, *318*, 269–271.

Schwartz, S. J., G. Paschmann, N. Sckopke, T. M. Bauer, M. Dunlop, A. N. Fazakerley, and M. F. Thomsen (2000), Conditions for the formation of hot flow anomalies at Earth's bow shock, *J. Geophys. Res.*, *105*(A6), 12,639–12,650.

Sibeck, D. G., R. E. Lopez, and E. C. Roelof (1991), Solar wind control of the magnetopause shape, location, and motion, *J. Geophys. Res.*, *96*, 5489–5495.

Sibeck, D. G., et al. (1999), Comprehensive study of the magnetospheric response to a hot flow anomaly, *J. Geophys. Res.*, *104*(A3), 4577–4593.

Sonnerup, B. U. Ö., and M. Guo (1996), Magnetopause transects, *Geophys. Res. Lett.*, *23*, 3679–3682.

Sonnerup, B. U. Ö., and M. Scheible (1998), Minimum and maximum variance analysis, in *Analysis Methods for Multi-spacecraft Data*, edited by G. Paschmann and P. W. Daly, chap. 8, pp. 185–220, Int. Space Sci. Inst., Bern, Switzerland.

Sonnerup, B. U. Ö., H. Hasegawa, W.-L. Teh, and L.-N. Hau (2006), Grad-Shafranov reconstruction: An overview, *J. Geophys. Res.*, *111*, A09204, doi:10.1029/2006JA011717.

Sonnerup, B. U. Ö., W.-L. Teh, and H. Hasegawa (2008), Grad-Shafranov and MHD reconstructions, in *Multi-spacecraft Analysis Methods Revisited, Rep. ISSI SR-008*, edited by G. Paschmann and P. W. Daly, pp. 81–90, Eur. Space Agency, Paris.

Thomsen, M. F., J. T. Gosling, S. A. Fuselier, S. J. Bame, and C. T. Russell (1986), Hot, diamagnetic cavities upstream from the Earth's bow shock, *J. Geophys. Res.*, *91*(A3), 2961–2973.

Thomsen, M. F., V. A. Thomas, D. Winske, J. T. Gosling, M. H. Farris, and C. T. Russell (1993), Observational test of hot flow anomaly formation by the interaction of a magnetic discontinuity with the bow shock, *J. Geophys. Res.*, *98*(A9), 15,319–15,330, doi:10.1029/93JA00792.

Wilken, B., et al. (2001), First results from the RAPID imaging energetic particle spectrometer on board Cluster, *Ann. Geophys.*, *19*, 1355–1366.

Zhang, H., et al. (2010), Time history of events and macroscale interactions during substorms observations of a series of hot flow anomaly events, *J. Geophys. Res.*, *115*, A12235, doi:10.1029/2009JA015180.